Journal of Nuclear Materials 527 (2019) 151790

Contents lists available at ScienceDirect

Journal of Nuclear Materials

journal homepage: www.elsevier.com/locate/jnucmat

Additional complexity in the Raman spectra of U_3O_8 ☆

A. Miskowiec*, J.L. Niedziela, T.L. Spano, M.W. Ambrogio, S. Finkeldei, R. Hunt, A.E. Shields

Oak Ridge National Laboratory, Oak Ridge, TN, 37831, USA

HIGHLIGHTS

- U_3O_8 has strong, low-energy Raman-active modes.
- Defect driven phonon lifetime suppression may be present in U_3O_8.
- Detailed peak fitting analysis may suggest subtle differences in spectra correlated with oxidation.

GRAPHICAL ABSTRACT

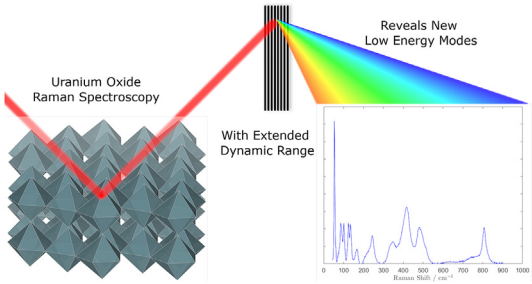

ARTICLE INFO

Article history:
Received 25 July 2019
Received in revised form
4 September 2019
Accepted 5 September 2019
Available online 10 September 2019

Keywords:
Raman spectroscopy
Uranium oxides
U_3O_8

ABSTRACT

Uranium oxides are readily amenable to investigation using Raman spectroscopy, and this technique is frequently used as a chemical analysis tool. We show, in triuranium octoxide (U_3O_8), the presence of previously unreported Raman peaks located below 100 cm^{-1}. By maximum intensity, the strongest peak in U_3O_8 appears at 54 cm^{-1} and is resolution limited, making this mode an ideal candidate for chemically identifying U_3O_8 using Raman spectroscopy. Detailed peak analysis indicates that the main spectral feature between 300 and 500 cm^{-1} is more accurately described by a septet than a triplet. Two samples of differing oxygen content show only minor differences in bulk crystal structure, but subtle changes in lattice dynamics are suggestive of defect scattering in analogy to UO_{2+x}.

1. Introduction

Raman spectroscopy has been used for identifying chemical composition of uranium oxides with great success [1–3]. In addition to probing fundamental information about the lattice dynamics of materials, Raman spectroscopy with microscopy (μ-Raman spectroscopy) has been shown to be a useful chemical identification and analysis tool [3–5]. Because of its ubiquity as a stable oxide form at room temperature, triuranium octoxide (U_3O_8) is a critically important oxide form for nuclear materials, geology, and forensics, and consequently the Raman spectra of U_3O_8 has been investigated by many authors [1,2,4–10]. We extend these previous works by employing high-resolution μ-Raman spectroscopy on samples of α-U_3O_8. We use a high-resolution notch filter with a band cutoff equivalent to a Raman shift of 45 cm^{-1} to extend the dynamic range of spectral interrogation below the common $\approx$100 cm^{-1} limit.

U_3O_8 was prepared by calcination of UO_2 (natural isotopic

☆ This manuscript has been authored by UT-Battelle, LLC, under contract DE-AC05- 00OR22725 with the US Department of Energy (DOE). The US government retains and the publisher, by accepting the article for publication, acknowledges that the US government retains a nonexclusive, paid-up, irrevocable, worldwide license to publish or reproduce the published form of this manuscript, or allow others to do so, for US government purposes. DOE will provide public access to these results of federally sponsored research in accordance with the DOE Public Access Plan (http://energy.gov/downloads/doe-public-access-plan).

* Corresponding author.
E-mail address: miskowiecaj@ornl.gov (A. Miskowiec).

https://doi.org/10.1016/j.jnucmat.2019.151790
0022-3115/

composition) pellets in air in a Thermolyne 47900 furnace. Two samples are investigated in this work: one calcined for 60 m at 1323 K gained a mass equivalent to $U_3O_{7.600}$ ($\approx$ 80% oxidized) and a second calcined at 973 K for 180 m gained a mass equivalent to $U_3O_{7.980}$ ($\approx$ 99% oxidized). Hereafter these samples will be referred to as the low-oxidation sample (LOS) and high-oxidation sample (HOS). For powder x-ray diffraction, samples were prepared by manually pulverizing the powder before mounting on a zero-background silicon plate, mixed with NIST SRM 640e (Si line position standard), and measured on a Proto Mfg. AXRD benchtop x-ray diffractometer. Raman spectra were collected on a Renishaw inVia μ-Raman spectrometer with three laser lines: 532, 633, and 785 nm. We present data only from the 785 nm laser line, for which the instrument was equipped with the high-resolution filter, but no dispersive behavior was observed in any spectra. With the 785 nm laser, we used a 1200 lines/mm diffraction grating for analysis. Data presented here were collected through a Leica 25 mm, 50$\times$ optical objective. The average spectral resolution in the region of interest (0–900 cm^{-1}) is $\approx$3 cm^{-1}. Raman spectra were background subtracted using an asymmetric least-squares algorithm with $p = 100{,}000$ and $\lambda = 0.0015$ prior to fitting [12]. Peak locations were determined by multipeak fitting using the *lmfit* module as implemented in the *PeakFitGUI* package written by one of the authors [13,14]. Discrimination of models with different numbers of peaks was done by comparing the Akaike information criterion [15]. A symmetry analysis indicates that all 30 optical phonons in α-U_3O_8 are Raman active.

In Fig. 1 we present x-ray diffraction patterns of LOS and HOS. Phase identification was done via Rietveld refinement: some fraction of β-U_3O_8 was observed in both samples (HOS: 27.4 mmolβ/molα; LOS: 58.7 mmolβ/molα) [16]. General agreement is observed between lattice constants in HOS and LOS in Table 1 with the reported values of α-U_3O_8 in the *Amm*2 space group as reported by Loopstra [11]. No discernible differences in lattice constants between HOS and LOS are observed. Although our value of *b* would appear to be lower than previous measurements, 11.95 Å is within the historically observed range for U_3O_8 [17].

Fig. 2 shows as-counted Raman spectra of LOS and HOS collected at room temperature. Major features include a triplet of bands in the 300–500 cm^{-1} region, a broad spectral feature near 807 cm^{-1}, a quartet of modes between 90 and 150 cm^{-1} and, most importantly, previously unreported resolution-limited modes at low energy. Below 100 cm^{-1}, a typical Raman energy cutoff, two intense modes at 54 and 87 cm^{-1} are observed. The 54 cm^{-1} mode, in particular, is noteworthy because it shows the narrowest linewidth of any peak (2 cm^{-1} Gaussian width) and has the highest peak counts and therefore highest signal-to-noise ratio. To our knowledge, this

Table 1
Refined lattice constants of HOS and LOS α-U_3O_8.

	a	b	c
	Å	Å	Å
HOS	4.14 (8)	11.95 (1)	6.72 (7)
LOS	4.14 (7)	11.95 (1)	6.72 (2)
Loopstra [11]	4.148	11.968	6.717

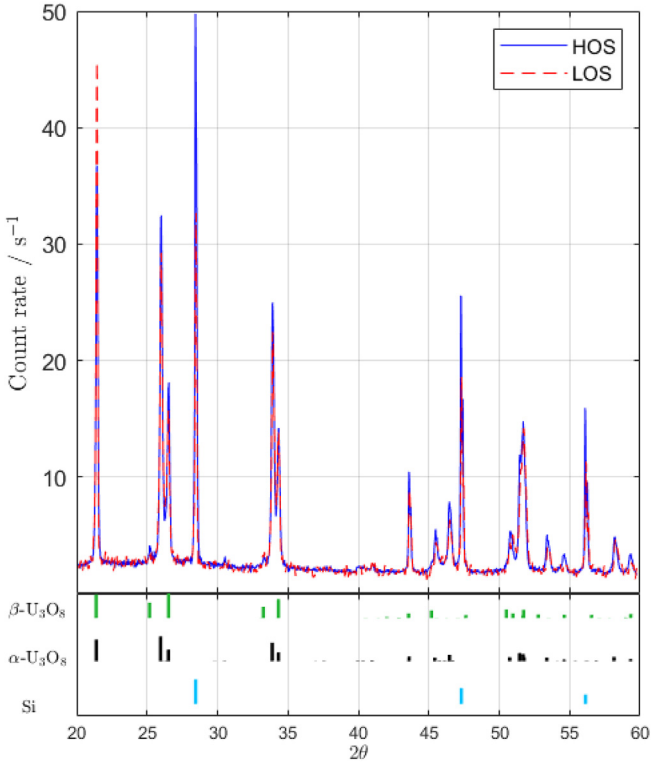

Fig. 1. X-ray diffraction pattern of (blue) HOS and (red) LOS α-U_3O_8 collected with CuK$_\alpha$ radiation. A small fraction of β-U_3O_8 was observed in both samples, but the majority phase fraction is *Amm*2 α-U_3O_8 [11]. (For interpretation of the references to colour in this figure legend, the reader is referred to the Web version of this article.)

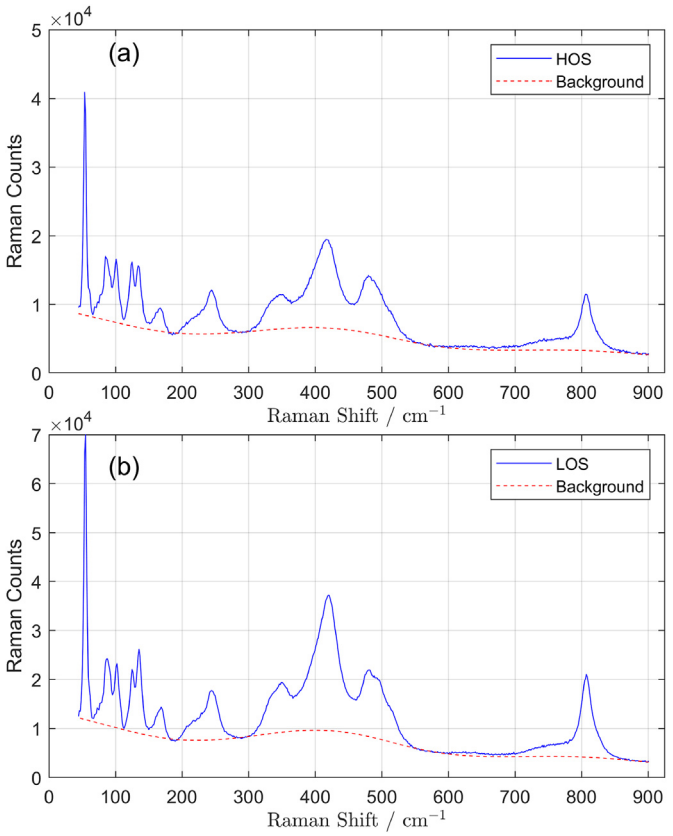

Fig. 2. Raw Raman spectra of (a) HOS and (b) LOS α-U_3O_8. Data were collected over the course of 1 h at an input 785 nm laser power of 1.5 μW, corresponding to a power density of 100 W/cm^2, through a 25 mm working length 50$\times$ optical objective (NA = 0.5). Photon count uncertainty (not shown) is approximately the width of plotted lines. Dashed red lines show calculated background term using an asymmetric least-squares algorithm with $p = 10^6$ and $\lambda = 1.5 \times 10^{-3}$. (For interpretation of the references to colour in this figure legend, the reader is referred to the Web version of this article.)

mode has not yet been reported in the literature. Collectively, the five modes below 150 cm^{-1} are a strong candidate for spectral identification due to their narrowness. The narrowness of these peaks also indicate that they are not of electronic origin (i.e., fluorescence), which must be significantly broader, and their intensities are not commensurate with possible atmospheric scattering (nor do measurements of the same beam path without a sample show an excitation at 54 cm^{-1}). Other possible sources of artifact scattering include cosmic rays and "hot" pixels, which can be excluded due to the peak width (larger than one CCD pixel). Thus, the 54 cm^{-1} mode cannot plausibly be explained by experimental artifacts.

The triplet feature near 300–500 cm^{-1} has previously been used as a defining chemical feature in U_3O_8. After background subtraction (Fig. 3), it is clear that LOS and HOS show only small differences. No significant shifts in peak location are observed between samples, and intensity variations of some peaks (90, 100, 112, 350, 415, and 807 cm^{-1} show intensity differences) are minor. This observation is in strict contrast to the case of the fluorite-structured actinides UO_2 and PuO_2, in which significant shifts in both spectral position and intensity as a function of oxidation (*i.e.*, x in $[Ac]O_{(2+x)}$, [Ac] = U or Pu) have been observed [18,19]. In the fluorite actinides, additional oxygens are accommodated by interstitial sites, activating a defect-mediated Raman mode and causing a decrease in lattice parameter and a hardening of the T_{2g} mode in response. In U_3O_8, suboxidation occurs such that oxygen vacancies are expected. The details of oxygen vacancy locations in U_3O_8 are not yet fully understood, but a commensurately simple relationship with lattice structure and dynamics apparently does not present itself [20].

Detailed peak fitting was performed for LOS and HOS (Fig. 4), with results tabulated in Table 2 and compared to previously reported literature values. In Table 2, the parameters are given by

$$F(x,A,\mu,\sigma,\alpha) = \frac{(1-\alpha)A}{\sigma\sqrt{2\pi}}\exp\left[-(x-\mu)^2/2\sigma^2\right] + \frac{\alpha A}{\pi}\left[\frac{\sigma_L}{(x-\mu)^2+\sigma_L^2}\right], \quad (1)$$

where $\sigma_L = \sqrt{2\ln(2)}\sigma$, α is the Lorentzian fraction, A is the amplitude, μ is the peak center position, and σ is the Gaussian width. Full spectral fitting reveals that the triplet of modes between 300 and 550 cm^{-1} is more accurately described as multiplet of at least 7 modes. While the 420 cm^{-1} mode in the LOS sample is the strongest, the mode centered at 398 cm^{-1} has more total counts in the HOS sample. In fact, the change in intensity of the 420 cm^{-1} mode (418.5 cm^{-1} in HOS) between HOS and LOS is the most apparent difference between those samples. To wit, this mode contains 80% more counts in LOS than in HOS (compared to the other peaks in the multiplet), and is significantly more Gaussian in nature ($\alpha = 0.14$ in HOS and $\alpha = 0.56$ in LOS).

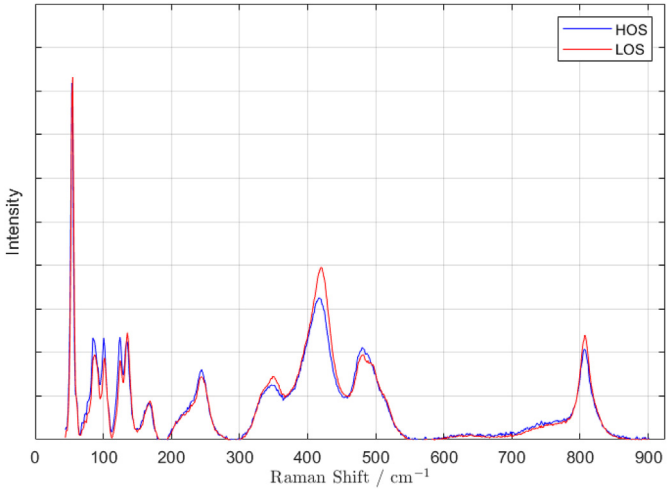

Fig. 3. Background subtracted Raman spectra for (blue) HOS and (red) LOS α-U_3O_8, normalized to total counts after background subtraction. LOS U_3O_8 shows slightly enhanced intensity of the 350, 415, and 810 cm^{-1} peaks, and slightly lower intensity of 90, 100, and 112 cm^{-1} peaks. Overall, the differences in Raman spectra from LOS and HOS α-U_3O_8 are minor, in contrast to UO_2 or PuO_2, for instance Refs. [18,19]. (For interpretation of the references to colour in this figure legend, the reader is referred to the Web version of this article.)

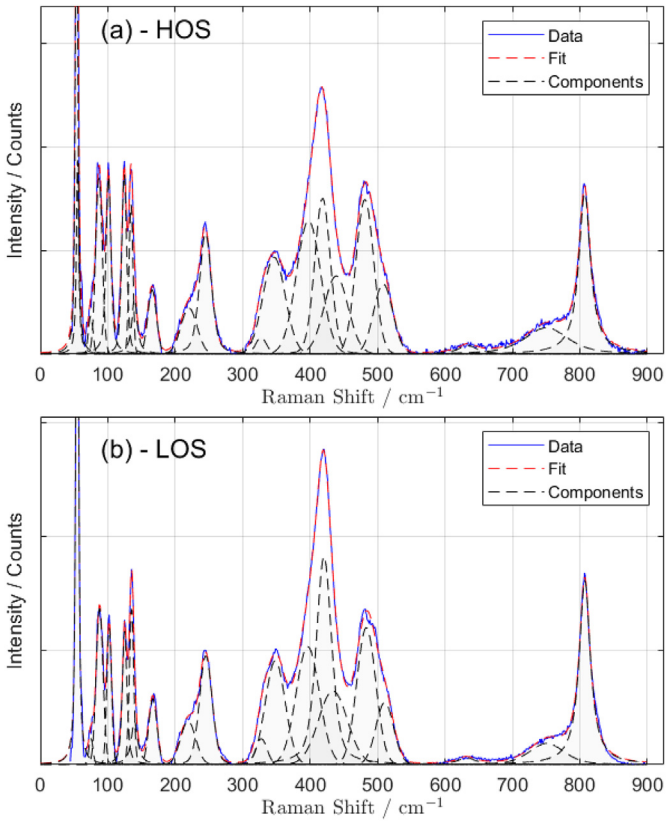

Fig. 4. Result of peak fitting for (a) HOS and (b) LOS α-U_3O_8. Modeled here, U_3O_8 contains 21 pseudo-Voigt profiles. The ordinate is truncated to show additional detail.

Based on these facts, we speculate the 420 cm^{-1} mode may include a component originating from defect scattering. The Gaussian portion, dominant in the HOS, represents normal Raman scattering events. The Lorentzian component originates from oxygen vacancy defect scattering, in analogy to UO_2, and is stronger in the LOS case wherein the defect density is necessarily higher. All of the increase in intensity of the 420 cm^{-1} peak can be explained by an increase in counts originating from the Lorentzian component only. Although it is much weaker in intensity, the peak near 135 cm^{-1} shows the same pattern: an increase in intensity in the LOS relative to other peaks in the multiplet that can be attributed entirely to an increase in Lorentzian component.

Additional theoretical analysis, such as density functional theory calculations, would be required to examine this possibility. However, the lack of significant differences in lattice constants for HOS and LOS suggests that oxygen vacancies do not have a drastic impact on long-range structure. In UO_2, defect-driven overtone modes were observed [18]. Here, those overtones would be expected at 840 cm^{-1} but, if they exist, they could not be resolved in these data.

Table 2
Raman peak intensities, positions, widths, and Lorentzian fraction for HOS and LOS U_3O_8, as well as literature values for U_3O_8 peak intensities, positions, and widths. **Bold** = not previously reported. *Italic* = not previously observed. For referenced values, * indicates our own determination - s = strong, m = moderate, w = weak, n = narrow, br = broad, sh = shoulder. Entries that have been observed but not reported do not have previous spectral assignments.

HOS				LOS				Literature			
Rel. Inten	Center	Width	Lor. Frac	Rel. Inten	Center	Width	Lor. Frac	Center	Amplitude	Width	Ref.
54	***53.7***	1.8	0.74	61.0	***54.6***	2	0.71				
20	***55.1***	1.7	1	<1	*60.6*	25.9	0.81				
5	**74.6**	3.4	0	3	**74.9**	3.1	0				[21]
36	**86.9**	4.9	0	27	**87.8**	5.1	0				[21]
35	**101.0**	3.6	0.7	17	**102.1**	3.5	0.04				[21]
32	**124.3**	3.7	0.48	20	**125.0**	3.4	0.63				[21]
18	134.3	2.9	0	18	135.1	3.2	0.19	130	s*	n*	[8]
14	139.5	3.9	1	10	139.4	4.7	1				[1–4]
17	165.6	6.3	0.04	14	166.8	6.1	0	164	w*	m*	[3]
23	220.4	12.0	0	17	219.1	11.2	0	185	m*	n*	[1]
53	244.8	8.9	0.46	38	245.3	9.4	0.22	243	m	m*	[8]
5	327.2	8.0	0	7	327.6	8.4	0	343	m	m*	[2]
67	346.6	16.5	0	52	348.3	14.7	0	351	m	sh*	[2]
100	**397.7**	18.0	0	70	**396.5**	17.3	0.01				[1–4]
79	418.5	11.6	0.14	100	420.6	11.4	0.56	412	s	m*	[2]
58	**438.5**	17.8	0	54	**433.8**	21.4	0				[1–4]
85	481.2	13.2	0	66	483.3	14.1	0	483	s	m*	[2]
41	**508.3**	14.2	0	28	**510.6**	13.1	0				[1–4]
8	633.7	14.6	1	5	632.1	13.8	0.94	638	w	m*	[4]
45	750.3	32.5	0.66	22	751.0	26.2	0.45	738	m	br*	[2]
87	807.1	8.8	1	79	807.3	8.4	1	811	s	n*	[2]

Proper fitting of the spectra in U_3O_8 reveals subtle changes in peak character that may be indicative of defect scattering in the strong multiplet between 300 and 550 cm^{-1}. In addition, the low-energy regime ($< 100\ cm^{-1}$) shows the presence of several additional peaks with high signal-to-noise ratio. In UO_2, the position and intensity of defect bands is systematically related to the stoichiometry. Here, we show that such a correlation may exist for U_3O_8 as well, but that a careful analysis is needed due to the larger number of Raman active modes in the U_3O_8 structure.

Data availability

The raw and processed data required to reproduce these findings are available upon request to the corresponding author.

Appendix A. Supplementary data

Supplementary data to this article can be found online at https://doi.org/10.1016/j.jnucmat.2019.151790.

References

[1] F. Pointurier, O. Marie, Identification of the chemical forms of uranium compounds in micrometer-size particles by means of micro-Raman spectrometry and scanning electron microscope, Spectrochim. Acta B 65 (2010) 797–804, https://doi.org/10.1016/j.sab.2010.06.008.

[2] M.L. Palacios, S.H. Taylor, Characterization of uranium oxides using in situ micro-Raman spectroscopy, Appl. Spectrosc. 54 (2000) 1372.

[3] E.A. Stefaniak, A. Alsecz, I.E. Sajò, A. Worobiec, Z. Máthé, S. Török, R.V. Grieken, Recognition of uranium oxides in soil particulate matter by means of μ-Raman spectrometry, J. Nucl. Mater. 381 (2008) 278–283, https://doi.org/10.1016/j.jnucmat.2008.08.036.

[4] I.S. Butler, G.C. Allen, N.A. Tuan, Micro-Raman spectrum of triuranium octoxide, U3O8, Appl. Spectrosc. 42 (1988) 901–902.

[5] G.C. Allen, I.S. Butler, N.A. Tuan, Characterisation of uranium oxides by micro-Raman spectroscopy, J. Nucl. Mater. 144 (1987) 17–19.

[6] H. Idriss, Surface reactions of uranium oxide powder, thin films and single crystals, Surf. Sci. Rep. 65 (2010) 67–109, https://doi.org/10.1016/j.surfrep.2010.01.001.

[7] M.J. Lipp, Z. Jenei, J. Park Klepeis, W.J. Evans, Raman Investigation of the Uranium Compounds $U3O_8$, UF_4, UH_3, UO_3 under Pressure at Room Temperature, Lawrence Livermore National Laboratory, 2011, https://doi.org/10.2172/1034513. Report.

[8] D.M.L. Ho, D. Manara, P. Lindqvist-Reis, T. Fanghänel, K. Mayer, The use of different dispersive Raman spectrometers for the analysis of uranium compounds, Vib. Spectrosc. 73 (2014) 102–110, https://doi.org/10.1016/j.vibspec.2014.05.002.

[9] D.M.L. Ho, A.E. Jones, J.Y. Goulermas, P. Turner, Z. Varga, L. Fongaro, T. Fanghänel, K. Mayer, Raman spectroscopy of uranium compounds and the use of multivariate analysis for visualization and classification, Forensic Sci. Int. 251 (2015) 61–68, https://doi.org/10.1016/j.forsciint.2015.03.002.

[10] E.A. Stefaniak, F. Pointurier, O. Marie, J. Truyens, Y. Aregbe, In-SEM Raman microspectroscopy coupled with EDX–a case study of uranium reference particles, Analyst 139 (2014) 668–675, https://doi.org/10.1039/C3AN01872E.

[11] B.O. Loopstra, Neutron diffraction investigation of U_3O_8, Acta Crystallogr. 17 (1964) 651–654, https://doi.org/10.1107/S0365110X6400158X.

[12] P.H.C. Eilers, H.F.M. Boelens, Baseline Correction with Asymmetric Least Squares Smoothing, Leiden University Medical Centre, 2005. Report.

[13] Newville, M., Otten, R., Nelson, A., Ingargiola, A., Stensitzki, T., Allan, D., Fox, A., Carter, F., Michal Pustakhod, D., Glenn, Ram, Y., MerlinSmiles Deil, C., Stuermer Beelen, A., Frost, O., gpasquev Hansen A. L. R., Stark, A., Spillane, T., Caldwell, S., Polloreno, A., andrewhannum Borreguero, J.M., Fraine, J., deep 42-thought, Maier, B. F., Gamari, B., Almarza, A., 2019. lmfit/lmfit-py 0.9.13 doi: 10.5281/zenodo.2620617.

[14] A. Miskowiec, Peakfitgui/peakfitgui 1.0, 2019, https://doi.org/10.11578/dc.20190904.1.

[15] H. Akaike, A new look at the statistical model identification, IEEE Trans. Autom. Control 19 (1974) 716–723, https://doi.org/10.1109/TAC.1974.1100705.

[16] B.H. Toby, EXPGUI, a graphical user interface for GSAS, J. Appl. Crystallogr. 34 (2001) 210–213, https://doi.org/10.1107/S0021889801002242.

[17] A.F. Andresen, The structure of U_3O_8 determined by neutron diffraction, Acta Crystallogr. 11 (1958) 612–614, https://doi.org/10.1107/S0365110X5800164X.

[18] J.M. Elorrieta, L.J. Bonales, N. Rodriguez-Villagra, V.G. Baonza, J. Cobos, A detailed Raman and x-ray study of UO_{2+x} oxides and related structure transitions, Phys. Chem. Chem. Phys. 18 (2016) 28209–28216, https://doi.org/10.1039/C6CP03800J.

[19] J.M. Elorrieta, D. Manara, L.J. Bonales, J.F. Vigier, O. Dieste, M. Naji, R.C. Belin, V.G. Baonza, R.J.M. Konings, J. Cobos, Raman study of the oxidation in (U, Pu)O_2 as a function of Pu content, J. Nucl. Mater. 495 (2017) 484–491, https://doi.org/10.1016/j.jnucmat.2017.08.043.

[20] R.J. Ackermann, A.T. Chang, C.A. Sorrell, Thermal expansion and phase transitions of the U_3O_{8-z} phase in air, J. Inorg. Nucl. Chem. 39 (1977) 75–85, https://doi.org/10.1016/0022-1902(77)80436-3.

[21] J.M. Elorrieta, L.J. Bonales, M. Naji, D. Manara, V.G. Baonza, J. Cobos, Laser-induced oxidation of UO2: a Raman study, J. Raman Spectrosc. 49 (2018) 878–884, https://doi.org/10.1002/jrs.5347.